

Molecular Nanomagnet $\text{Cu}^{\text{II}}\text{Ni}^{\text{II}}\text{Cu}^{\text{II}}$ as Resource for Quantum Entanglement, Coherence, and Spin Squeezing

Azadeh Ghannadan¹, Hamid Arian Zad^{2,*}, Saeed Haddadi^{3,1},
Jozef Strečka², Zhirayr Adamyan^{4,5} and Vadim Ohanyan^{4,5}

¹*Saeed's Quantum Information Group, P.O. Box 19395-0560, Tehran, Iran*

²*Department of Theoretical Physics and Astrophysics, Faculty of Science,
P. J. Šafárik University, Park Angelinum 9, 041 54 Košice, Slovak Republic*

³*Faculty of Physics, Semnan University, P.O. Box 35195-363, Semnan, Iran*

⁴*Laboratory of Theoretical Physics, Yerevan State University, Alex Manoogian 1, 0025 Yerevan, Armenia*

⁵*CANDLE, Synchrotron Research Institute, 31 Acharyan Str., 0040 Yerevan, Armenia*

(Dated: July 10, 2024)

We investigate key quantum characteristics of the mixed spin-(1/2,1,1/2) Heisenberg trimer under the influence of an external magnetic field. Specifically, we analyze the distributions of bipartite and tripartite entanglement quantified through the respective negativities, the l_1 -norm of coherence, and spin squeezing with the help of rigorous analytical and numerical methods. Our findings suggest that the heterotrimeric molecular nanomagnet $[\{\text{Cu}^{\text{II}}\text{L}\}_2\text{Ni}^{\text{II}}(\text{H}_2\text{O})_2](\text{ClO}_4)_2\cdot 3\text{H}_2\text{O}$, which represents an experimental realization of the mixed spin-(1/2,1,1/2) Heisenberg trimer, exhibits a significant bipartite entanglement between Cu^{II} and Ni^{II} magnetic ions along with robust tripartite entanglement among all three constituent magnetic ions. The significant bipartite and tripartite entanglement persists even at relatively high temperatures up to 37 K and magnetic fields up to 50 T, whereby the coherence is maintained even at elevated temperatures. In addition, we investigate the spin squeezing parameter within thermal states of the spin-(1/2,1,1/2) Heisenberg trimer. Our exact results reveal optimal conditions for achieving the highest degree of the spin squeezing, which are achieved at zero magnetic field around $T \approx 30$ K.

I. INTRODUCTION

Entanglement [1], a cornerstone of quantum mechanics, plays a crucial role in the study of molecular magnets [2, 3], driving advancements in quantum information and condensed matter physics [4–6]. In this context, Heisenberg spin clusters serve as exemplary systems for exploring fundamental quantum properties, such as entanglement [7–10], quantum coherence [11–13], and spin squeezing [14–19]. These properties not only illuminate the intricate behavior of quantum systems but also pave the way for practical applications in quantum information [19–23], magnetic resonance [24] and improving the sensor sensitivity [25–27]. Our investigation is particularly inspired by the experimental developments in molecular magnets, which provide a tangible platform for testing theoretical predictions. By studying the quantum characteristics of Heisenberg spin clusters, we aim to deepen our understanding of these phenomena and their implications for future quantum technologies [1, 5].

Different states coexist simultaneously through superposition in quantum systems, which is known as quantum coherence [28]. Many quantum technologies including cryptography and computing depend on this feature. It is well known that real systems can exhibit interference effects when they are coherent, which makes it easier to accurately control and manipulate their behavior. However, coherence is brittle and easily disrupted by

interactions with the surroundings, leading to decoherence [29, 30]. As such maintaining coherence is a significant obstacle to the development of useful quantum technologies. Generally speaking, the quantum coherence of real systems is affected by various factors, including environmental noise and general decoherence mechanisms [31, 32]. Indeed, the environmental noise caused by some factors such as thermal fluctuations can disrupt the fragile quantum superpositions required for coherence. Thus, studying quantum coherence is crucial for exploring the quantum characteristics of these systems under decoherence.

According to the hierarchy of quantum resources [33], quantum coherence and entanglement are different but related phenomena (quantum coherence \supseteq entanglement), and they serve distinct purposes in quantum information processing. Quantum coherence, as mentioned earlier, refers to the ability of a quantum system to exist in a superposition of states, meaning that it can be in multiple states simultaneously. This property is vital for some interesting tasks like quantum communication and quantum computation, where controlling and preserving coherence is crucial for performing complex calculations or transmitting information securely [34–36]. Entanglement, on the other hand, is a special kind of correlation that exists between the states of two or more quantum systems, where the states of each system are intrinsically linked, even when they are physically separated. In some cases, depending on the specific application, examining quantum coherence may be preferred over entanglement. Therefore, the reason to choose quantum coherence over entanglement (or vice versa) depends on the requirements

* Corresponding author: hamid.arian.zad@upjs.sk

of the considered quantum protocol or program, as well as specific constraints and resources.

Theoretical advancements over the past two decades have deepened our understanding of spin squeezing [14, 37–40], from its creation by interactions in optical lattices [41–43] and Rydberg atoms [44] to its application in programmable quantum sensors [25–27]. A coherent spin state is defined as a minimum-uncertainty state where all components of the collective spin operator of an ensemble of spinful particles have the same variance. Spin squeezing refers to the redistribution of quantum fluctuations in such a state, resulting in the variance of one spin component being smaller than that of the other components. This phenomenon allows for measurements that surpass the shot-noise limit, facilitating high-precision measurements, and the generation of many-body entangled and many-body Bell correlated states [38, 39].

The study and experimental use of spin squeezing in spin models have garnered significant interest in recent years [45]. In quantum metrology [46–48], spin squeezing has been employed to improve atomic precision measurements beyond the standard quantum limit [49, 50], which is defined as the maximum phase sensitivity achievable with separable states. This advancement has important implications for various technologies, including Ramsey spectroscopy [51–53], quantum interferometer [27, 54] and atomic clocks [55, 56]. By enhancing the accuracy of measurements, spin squeezing contributes to the development of more precise measurement devices.

In the present work, we investigate the mixed-spin (1/2,1,1/2) Heisenberg trimer, which can be experimentally realized by the heterotrimeric molecular nanomagnet $\{[\text{Cu}^{\text{II}}\text{L}]_2\text{Ni}^{\text{II}}(\text{H}_2\text{O})_2\}(\text{ClO}_4)_2 \cdot 3\text{H}_2\text{O}$ hereafter referred to as the $\text{Cu}^{\text{II}}\text{Ni}^{\text{II}}\text{Cu}^{\text{II}}$ molecular complex. The magnetic properties of the $\text{Cu}^{\text{II}}\text{Ni}^{\text{II}}\text{Cu}^{\text{II}}$ complex characterized by a linear structure and a rather weak single-ion anisotropy were studied in Ref. [57], where the strength of the exchange coupling between Cu^{II} and Ni^{II} ions were reported along with the single-ion anisotropy of the Ni^{II} ions.

In an earlier work [58], the magnetic properties of the $\text{Cu}^{\text{II}}\text{Ni}^{\text{II}}\text{Cu}^{\text{II}}$ complex were studied without considering single-ion anisotropy. Later, Hari *et al.* [59] synthesized and characterized a $\text{Cu}^{\text{II}}\text{Ni}^{\text{II}}\text{Cu}^{\text{II}}$ complex with nonzero $\text{Cu} \cdots \text{Cu}$ exchange coupling, which was found to be much smaller than the $\text{Cu} \cdots \text{Ni}$ exchange couplings. They then investigated its magnetic properties. Comparing the results obtained for the magnetic behavior of the two structural models—one with and one without $\text{Cu} \cdots \text{Cu}$ exchange coupling—it was observed that the magnetization and magnetic susceptibility behavior did not change significantly. In a very recent theoretical work [60], the ground-state phase diagram, bipartite entanglement, and magnetization properties of a trimeric model similar to that reported in Ref. [59], but with different Landé g -factors of Cu^{II} and Ni^{II} ions, have been investigated in detail.

Motivated by the results reported in Ref. [57], we se-

lected the $\text{Cu}^{\text{II}}\text{Ni}^{\text{II}}\text{Cu}^{\text{II}}$ complex without $\text{Cu} \cdots \text{Cu}$ exchange interaction to investigate the effects of the applied magnetic field and temperature on its quantum properties. This study provides a comprehensive examination of mixed spin-(1/2,1,1/2) Heisenberg trimer model with nonzero single-ion anisotropy in the presence of an external magnetic field, offering novel quantum insights that have not been previously explored in this context.

The structure of the paper is as follows: In Sec. II, we present the model and derive its partition function from the exact solution. Section III outlines the key formulas and theoretical approaches used in our analysis of the global density matrix of the system, as well as two reduced density matrices for a nonzero value of the single-ion anisotropy of the spin integer particle. This section also explores the tripartite entanglement negativity and two bipartite negativities with respect to the temperature and magnetic field. In Sec. IV we study the quantum coherence of the system and compare it with the entanglement negativities. The results, including numerical plots illustrating the thermal evolution of the spin squeezing parameter, are discussed in Sec. V. Finally, Sec. VII provides a summary and outlook.

II. MODEL

Let us consider the mixed spin-(1/2,1,1/2) Heisenberg trimeric cluster, which is experimentally motivated by the heterotrimeric $\text{Cu}^{\text{II}}\text{Ni}^{\text{II}}\text{Cu}^{\text{II}}$ complex. The model can be described by the Hamiltonian:

$$\hat{H} = J(\hat{s}_a \cdot \hat{S}_b + \hat{S}_b \cdot \hat{s}_c) + D(\hat{S}_b^z)^2 - g\mu_B B(\hat{s}_a^z + \hat{S}_b^z + \hat{s}_c^z). \quad (1)$$

Here, the first term of the Hamiltonian (1) expresses the nearest-neighbor exchange interactions between the spin operators \hat{s}_a and \hat{s}_c assigned to Cu atoms and the spin operator \hat{S}_b assigned to the Ni atom respectively, with the antiferromagnetic coupling constant $J > 0$. The second term refers to the single-ion anisotropy of the Ni atom with constant D . Finally, there is a Zeeman term, where μ_B is the Bohr magneton, g is the Landé g -factor and B is the static magnetic field applied along the z -axis. The Hamiltonian (1) can be solved analytically through the exact diagonalization method and a full set of eigenvalues and eigenvectors can be obtained. The twelve energy eigenvalues and their corresponding eigenvectors, written in standard bases of Hilbert space $|\phi\rangle = |s_a^z, S_b^z, s_c^z\rangle$ are given in Table I and the probability amplitudes of the eigenvectors are given in Appendix A. Next, the Gibbs free energy of the system can be calculated using the following expression:

$$\mathcal{G} = -k_B T \ln Z, \quad (2)$$

where Z is the partition function of the system that can be explicitly obtained from the sum of the exponentials

of the eigenenergies as:

$$\begin{aligned}
Z &= \sum_{i=1}^{12} \exp(-\beta E_i) = 1 + 2 \cosh(\beta h) \exp(-\beta D) \\
&+ \exp(-\beta(D-J)) + 2 \cosh(2\beta h) \exp(-\beta(D+J)) \\
&+ 4 \cosh(\beta h) \exp\left(-\frac{\beta D}{2}\right) \cosh\left(\frac{\beta}{2}\sqrt{D^2+4J^2}\right) \\
&+ 2 \cosh\left(\frac{\beta}{2}\sqrt{(D-J)^2+8J^2}\right) \exp\left(-\frac{\beta}{2}(D-J)\right). \quad (3)
\end{aligned}$$

Here, $\beta = 1/(k_B T)$, k_B is being the Boltzmann constant and T is the absolute temperature. For convenience, we introduced a new parameter $h = g\mu_B B$ representing the Zeeman term related to the applied magnetic field. Using the Gibbs free energy (2), we can derive other quantities such as magnetization:

$$M = -\frac{\partial \mathcal{G}}{\partial B}. \quad (4)$$

III. THE DENSITY MATRICES AND ENTANGLEMENT MEASURES

Having accomplished the eigenvalue problem of the mixed spin-(1/2,1,1/2) Heisenberg trimer and having the partition function in hand, one can step forward to evaluation of the density matrix which allows the calculation of bipartite and tripartite entanglement via a measure of negativity. As the first step, the overall density operator is defined by the formula:

$$\hat{\rho} = \frac{1}{Z} \exp(-\beta \hat{H}) = \frac{1}{Z} \sum_{i=1}^{12} \exp(-\beta E_i) |\psi_i\rangle \langle \psi_i|, \quad (5)$$

and the density matrix corresponding to the density operator in the standard basis $|\phi\rangle$ is written.

Then, to evaluate the bipartite entanglement between any spin pair, one should follow the calculation of the reduced density operator related to the spin pair by tracing out the degrees of freedom of the remaining spin of the mixed spin-(1/2,1,1/2) Heisenberg cluster. Although the reduced density operators $\hat{\rho}_{ab}$ and $\hat{\rho}_{bc}$ are not equivalent, the results of the negativity (as well as coherence) are identical, namely $N_{ab} = N_{bc}$. Therefore, hereafter the bipartite entanglement of parties s_a and S_b will be considered that is given by:

$$\hat{\rho}_{ab} = \text{Tr}_{s_c} \hat{\rho} = \frac{1}{Z} \sum_{i=1}^{12} \sum_{s_c^z = \pm 1/2} \exp(-\beta E_i) \langle s_c^z | \psi_i \rangle \langle \psi_i | s_c^z \rangle. \quad (6)$$

In a similar way, the reduced density operator relevant to s_a and s_c is calculated by tracing out the degrees of freedom of S_b :

$$\hat{\rho}_{ac} = \text{Tr}_{S_b} \hat{\rho} = \frac{1}{Z} \sum_{i=1}^{12} \sum_{S_b^z = 0, \pm 1} \exp(-\beta E_i) \langle S_b^z | \psi_i \rangle \langle \psi_i | S_b^z \rangle. \quad (7)$$

The next step is to write the matrix form of the reduced density operators and partially transpose them with respect to one of the spins of their basis. The elements of the partially transposed density matrices ρ_{ab} and ρ_{ac} are written as follows respectively:

$$\begin{aligned}
\langle s_a^{z'}, S_b^{z'} | \rho_{ab} | s_a^z, S_b^z \rangle^{T_a} &= \langle s_a^z, S_b^{z'} | \rho_{ab} | s_a^{z'}, S_b^z \rangle, \\
\langle s_a^{z'}, s_c^{z'} | \rho_{ac} | s_a^z, s_c^z \rangle^{T_c} &= \langle s_a^{z'}, s_c^z | \rho_{ac} | s_a^z, s_c^{z'} \rangle. \quad (8)
\end{aligned}$$

Ultimately, the bipartite negativities N_{ab} and N_{ac} measuring the magnitude of entanglement between the spin pairs s_a - S_b and s_a - s_c are calculated according to the formula by Vidal and Werner [61] that originates from the Peres-Horodecki separability criterion [62]:

$$N_{ab} = \sum_{i=1}^6 \frac{|\lambda_i| - \lambda_i}{2}, \quad N_{ac} = \sum_{i=1}^4 \frac{|\lambda_i| - \lambda_i}{2}, \quad (9)$$

where λ_i are the eigenvalues of the respective partially transposed density matrices. Both of the negativities N_{ab} and N_{ac} are calculated analytically and the possible negative eigenvalues that contribute to N_{ab} and N_{ac} are presented in Appendix B.

The tripartite entanglement of the mixed spin-(1/2,1,1/2) Heisenberg cluster is quantified through the tripartite negativity, which is calculated from the three different partial transposes of the overall density matrix. The first partial transpose of the overall density matrix with respect to the first spin of the basis ρ^{T_a} is performed by fixing the quantum numbers S_b^z and s_c^z in the basis $|s_a^z, S_b^z, s_c^z\rangle$ and interchanging quantum number s_a^z . The same pattern is repeated to obtain the partial transpose of the overall density matrix with respect to the second and third spins of the basis:

$$\begin{aligned}
\langle s_a^{z'}, S_b^{z'}, s_c^{z'} | \rho | s_a^z, S_b^z, s_c^z \rangle^{T_a} &= \langle s_a^z, S_b^{z'}, s_c^{z'} | \rho | s_a^{z'}, S_b^z, s_c^z \rangle, \\
\langle s_a^{z'}, S_b^{z'}, s_c^{z'} | \rho | s_a^z, S_b^z, s_c^z \rangle^{T_b} &= \langle s_a^{z'}, S_b^z, s_c^{z'} | \rho | s_a^z, S_b^{z'}, s_c^z \rangle, \\
\langle s_a^{z'}, S_b^{z'}, s_c^{z'} | \rho | s_a^z, S_b^z, s_c^z \rangle^{T_c} &= \langle s_a^{z'}, S_b^{z'}, s_c^z | \rho | s_a^z, S_b^z, s_c^{z'} \rangle. \quad (10)
\end{aligned}$$

The bipartite negativities that are calculated from the partially transposed density matrices (10) are respectively denoted by N_{a-bc} , N_{b-ac} and N_{c-ab} such that $N_{I-JK} = \sum_{i=1}^{12} \frac{|\lambda_i| - \lambda_i}{2}$ with $I = a, b, c$ and $JK = bc, ac, ab$. Consequently, the tripartite negativity of the mixed spin-(1/2,1,1/2) Heisenberg trimer can be calculated as the geometric mean of the bipartite negativities [63]:

$$N_{abc} = \sqrt[3]{N_{a-bc} N_{b-ac} N_{c-ab}}. \quad (11)$$

The matrix forms of overall density matrix, reduced density matrices, and their partially transposed density matrices are presented in Appendix A.

Now, let us begin with a detailed analysis of the ground-state behavior of the mixed spin-(1/2,1,1/2) Heisenberg trimer in presence of a magnetic field. To proceed to the results, all interaction terms involved in

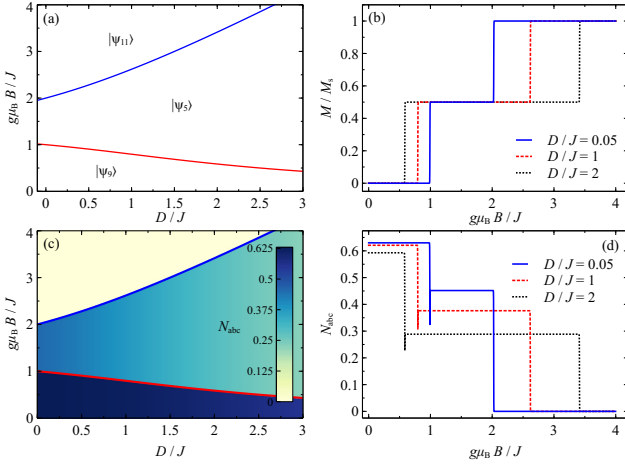


FIG. 1. (a) The ground-state phase diagram of the mixed spin-(1/2,1,1/2) Heisenberg trimer in the parameter space D/J vs. $g\mu_B B/J$; (b) The zero-temperature magnetization normalized with respect to the saturation value ($M_s = 2g\mu_B$) as a function of the magnetic field for three different values of the single-ion anisotropy D/J ; (c) The zero-temperature density plot of the tripartite negativity N_{abc} in the $g\mu_B B/J - D/J$ plane; (d) The tripartite negativity N_{abc} as a function of the magnetic field for three different values of D/J at zero temperature.

the Hamiltonian (1) will be normalized with respect to

the antiferromagnetic coupling constant $J > 0$, which will henceforth serve as an energy unit. The ground-state phase diagram of the mixed spin-(1/2,1,1/2) Heisenberg trimer is presented in Fig. 1(a) in the parameter space D/J vs. $g\mu_B B/J$. It turns out that there are three different ground states unambiguously given by the eigenvectors $|\psi_9\rangle$, $|\psi_5\rangle$ and $|\psi_{11}\rangle$ specifically quoted in Appendix A. The inspection of energy eigenvalues reveals the following phase boundaries between three available ground states $|\psi_9\rangle$, $|\psi_5\rangle$ and $|\psi_{11}\rangle$:

$$\begin{aligned} |\psi_5\rangle - |\psi_9\rangle : h &= \frac{J}{2} + \frac{1}{2} \left(\sqrt{(D-J)^2 + 8J^2} - \sqrt{D^2 + 4J^2} \right) \\ |\psi_{11}\rangle - |\psi_5\rangle : h &= J + \frac{D}{2} + \frac{1}{2} \sqrt{D^2 + 4J^2} \end{aligned} \quad (12)$$

In Fig. 1(b), the zero-temperature magnetization curves displaying zero, one-half and saturation plateaus are illustrated at three different cuts of the relevant ground state phase diagram. At low magnetic fields, the singlet ground state $|\psi_9\rangle$ having character of a quantum superposition of four basis states $|\downarrow 1 \downarrow\rangle$, $|\uparrow -1 \uparrow\rangle$, $|\uparrow 0 \downarrow\rangle$, and $|\downarrow 0 \uparrow\rangle$, with zero total spin moment $S_{\text{tot}}^z = 0$ is favored. This ground state corresponds to a zero magnetization plateau. At moderate magnetic fields, one contrarily encounters the triplet ground state $|\psi_5\rangle$ with character of a quantum superposition of three basis states $|\uparrow 1 \downarrow\rangle$, $|\downarrow 1 \uparrow\rangle$, $|\uparrow 0 \uparrow\rangle$ with the total spin moment $S_{\text{tot}}^z = 1$.

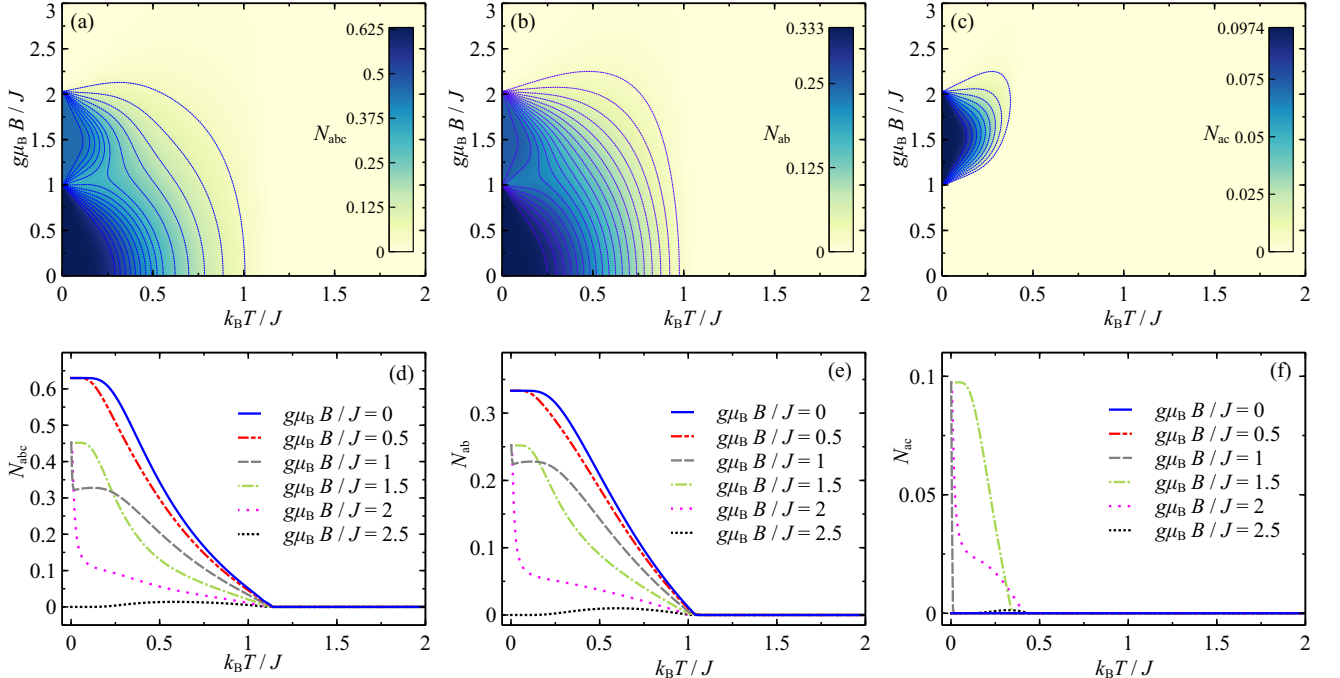


FIG. 2. (a) The tripartite negativity N_{abc} , (b) the bipartite negativity N_{ab} , and (c) the bipartite negativity N_{ac} of the mixed spin-(1/2,1,1/2) Heisenberg trimer in the $g\mu_B B/J - k_B T/J$ plane by assuming $D/J = 0.05$; (d) Temperature dependencies of the N_{abc} , (e) N_{ab} and (f) N_{ac} for a few selected values of the magnetic field and $D/J = 0.05$.

The ground state $|\psi_5\rangle$ thus corresponds to an intermediate one-half magnetization plateau being stable in

a rather wide region of the magnetic fields. Finally, one detects the fully saturated ground state $|\psi_{11}\rangle = |\uparrow 1 \uparrow\rangle$, which is reached at high enough magnetic fields where all three spins are fully aligned with the magnetic-field direction.

Fig. 1(c) displays the density plot of the tripartite negativity N_{abc} for the mixed spin-(1/2,1,1/2) Heisenberg trimer in the same parameter region as used in Fig. 1(a). As expected, the tripartite negativity is highest in the ground state $|\psi_9\rangle$ reaching a maximum value of $N_{abc} = 0.625$ at zero single-ion anisotropy. The singlet ground state $|\psi_9\rangle$ thus exhibits the most pronounced collective quantum features. In contrast, the collective quantum features are somewhat reduced within another quantum ground state $|\psi_5\rangle$ due to partial spin alignment towards the magnetic field realized in this one-half plateau state. Consequently, the tripartite negativity is substantially lower in the triplet ground state $|\psi_5\rangle$ in comparison with the singlet ground state $|\psi_9\rangle$. Finally, the tripartite negativity becomes zero in the fully polarized ground state $|\psi_{11}\rangle$. For better insight, the magnetic field variations of the tripartite negativity are shown in Fig. 1(d) for three different cuts of the relevant density plot. A prominent feature of single-ion anisotropy is the reduction of tripartite negativity, whereby this effect is much more pronounced for the triplet ground state $|\psi_5\rangle$ compared to the singlet ground state $|\psi_9\rangle$. It is also worth mentioning that there is a substantial drop in tripartite negativity at the phase boundary between $|\psi_9\rangle$ and $|\psi_5\rangle$, which relates to existence of a mixed state at the relevant phase boundary that reduces tripartite entanglement.

To provide a clear understanding of the thermal behavior of the mixed spin-(1/2,1,1/2) Heisenberg trimer, the density plot of tripartite as well as bipartite negativities are depicted in Fig. 2(a)-(c) for the particular case with the fixed value of single-ion anisotropy $D/J = 0.05$. It is quite clear that the magnetic-field-driven variations of the tripartite negativity N_{abc} at sufficiently low temperatures are in a perfect agreement with the abrupt changes of the tripartite negativity detected at zero temperature around the magnetic fields $g\mu_B B/J \approx 1$ and 2 [cf. Fig. 2(c)-(d)]. We note that, the tripartite negativity ranges from 0 to 1, where for our case its maximum is 0.625. It can be inferred from Figs. 2(b) and 2(c) that the bipartite negativities N_{ab} and N_{ac} form at low enough temperatures plateaus quite similarly as the tripartite negativity N_{abc} does. The tripartite negativity N_{abc} and the bipartite negativity N_{ab} display their highest achievable values, $N_{abc} = 0.625$ and $N_{ab} = 1/3$, in a low-field region inherent to the singlet ground state $|\psi_9\rangle$, whereas the maximum of bipartite negativity $N_{ac} \approx 0.0974$ can be found at moderate magnetic fields supporting the triplet ground state $|\psi_5\rangle$. Generally, the maximum values of both bipartite negativities are restricted to between 0 and 0.5. Absence of a direct exchange interaction between the corner spins s_a and s_c generally results in a lower value of the bipartite entanglement N_{ac} compared to the N_{ab} one assigned to directly interacting central

and corner spins. A gradual vanishing of tripartite and bipartite negativities is observed along the temperature axis in all three density plots shown in upper panel.

The bottom panel in Fig. 2 demonstrates typical temperature dependencies of the tripartite and bipartite negativities N_{abc} , N_{ab} and N_{ac} for a few selected values of the magnetic field. A common property of all temperature dependencies of tripartite and bipartite negativities in Fig. 2(d)-(f) is the gradual thermally-induced decline in the tripartite and bipartite entanglement. In Fig. 2(d) the tripartite negativity starts from its highest value $N_{abc} = 0.625$ achieved at zero magnetic field and vanishes at $k_B T/J \approx 1.15$. As the magnetic field strengthens, the initial value of the tripartite negativity gradually decreases, while the threshold temperature at which it becomes zero remains unchanged. Contrary to this, the negativity N_{ac} measuring the bipartite entanglement between the corner spins is zero at low magnetic fields, but starts from the initial value $N_{ac} \approx 0.0974$ at moderate magnetic fields $g\mu_B B/J \gtrsim 1$ and is rapidly suppressed upon increasing temperature terminating at the threshold temperature $k_B T/J \approx 0.4$ [see Fig. 2(e)]. The bipartite negativity N_{ab} follows trends similar to those of the tripartite negativity N_{abc} when reaching a maximum initial value $N_{ab} = 1/3$ and vanishing at the same threshold temperature $k_B T/J \approx 1.1$. A less pronounced reentrance in the tripartite and bipartite entanglement can be found at magnetic fields slightly exceeding the saturation value $g\mu_B B/J \gtrsim 2.5$ due to thermal excitations towards higher-energy levels. Besides, the peculiar changes in tripartite and bipartite entanglement observable around the magnetic fields $g\mu_B B/J \approx 1$ and 2 can be again attributed to the relevant magnetic-field-driven phase transitions.

IV. QUANTUM COHERENCE

There are several ways to evaluate quantum coherence [31]. Among these, the l_1 -norm of quantum coherence, which is widely used in quantum physics, has the following definition:

$$C = \sum_{i \neq j} |\rho_{i,j}|. \quad (13)$$

According to Eq. (13), the l_1 -norm of coherence can be expressed as the sum of absolute values of the off-diagonal elements corresponding to the selected basis [32].

To find more details regarding the quantum resources in the system under consideration, we have plotted the l_1 -norm of quantum coherence for the tripartite (C_{abc}) and bipartite (C_{ab} and C_{ac}) states in Fig. 3. As can be seen in Fig. 2, the tripartite and bipartite entanglement disappears at a certain threshold temperature, however, the quantum coherence of tripartite and bipartite states captured by l_1 -norm of coherence (13) remains nonzero even at higher temperatures as illustrated in Fig. 3(a)-(c) for a few selected values of the magnetic field and

$D/J = 0.05$. This result is expected because increasing temperature can reduce quantum correlations, such as entanglement, due to rising role of thermal fluctuations in the system. The quantum coherence can nevertheless remain a significant resource compared to entanglement based on the hierarchy of quantum resources [33] as the amount of entanglement is bounded by the quantum coherence [64]. It is worth noting that the qualitative behavior of quantum coherence is similar to that of entanglement, apart from some minor differences [compare Figs. 2(d)-(f) and 3(a)-(c)]. Moreover, despite the quantitative differences between tripartite and bipartite quantum coherences, their qualitative behavior is often the same, except for the bipartite coherence C_{ab} at low temperatures.

Fig. 3(d)-(f) shows the thermal coherence of the mixed spin-(1/2,1,1/2) Heisenberg trimer as a function of the magnetic field $g\mu_B B/J$ for a few selected values of temperature and one fixed value of the single-ion anisotropy $D/J = 0.05$. Regardless of temperature and single-ion anisotropy effects, one can see that the tripartite and bipartite quantum coherences decrease upon strengthening of the magnetic field. The only exception to this rule is

the l_1 -norm of the bipartite coherence C_{ac} , which displays a peculiar transient strengthening due to the magnetic field. In general, the suppression of thermal coherence by the magnetic field can be related to the Zeeman effect, which causes splitting of energy levels into sublevels (i.e. splitting of spin multiplets) and energetically favors the sublevels with the highest value of z -component of the total spin. As a result, the qualitative behavior of tripartite coherence [Fig. 3(d)] at zero and low temperatures is quite similar to the tripartite entanglement and magnetization [see blue lines in Figs. 1(b) and 1(d)]. The inclusion of a relatively small single-ion anisotropy may further cause zero-field splitting of energy levels and hence, it may additionally enhance the effect of external magnetic field. Altogether, the combined effect of magnetic field and single-ion anisotropy results in a more rapid loss of quantum coherence of the mixed spin-(1/2,1,1/2) Heisenberg trimer under thermal conditions. While the tripartite coherence and tripartite entanglement disappear at absolute zero temperature at the saturation field, it can be observed from Figs. 2 and 3 that increasing temperature can delay this disappearance for larger magnetic fields.

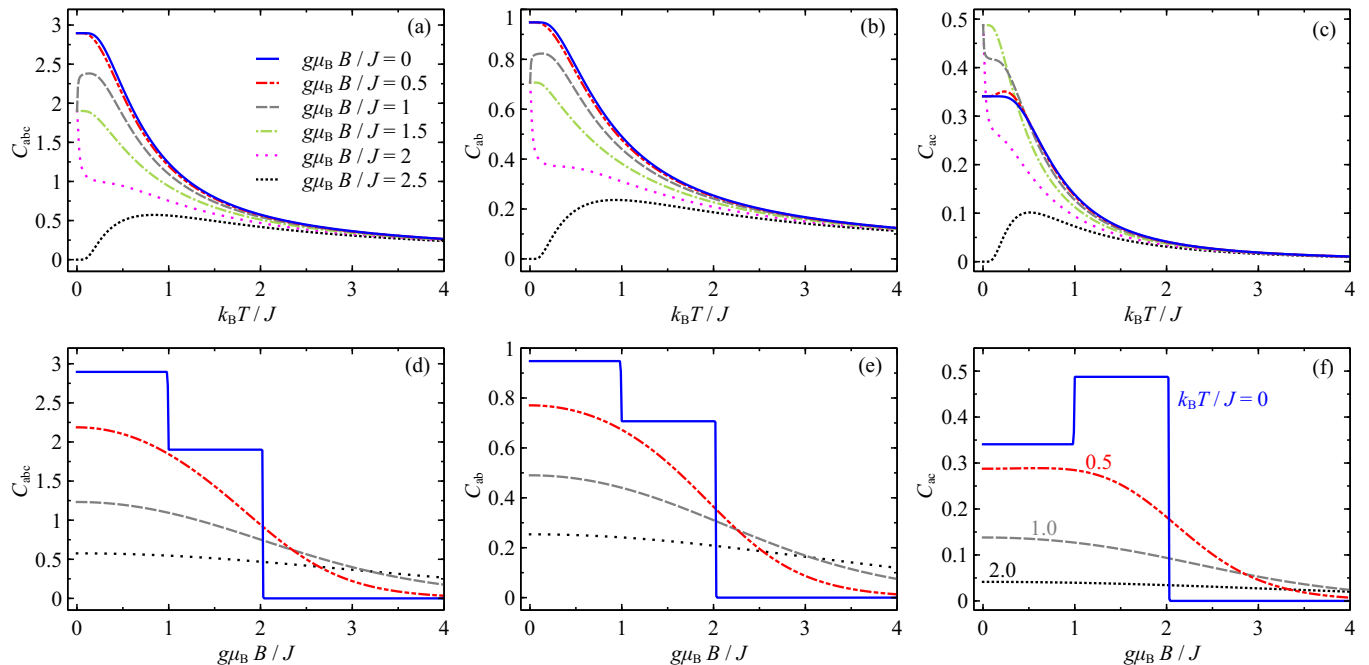


FIG. 3. (a)-(c) The temperature dependencies of the quantum coherence (tripartite and bipartite) of the mixed spin-(1/2,1,1/2) Heisenberg trimer for a few selected values of the magnetic field and one fixed value of the single-ion anisotropy $D/J = 0.05$, (d)-(f) the quantum coherence as a function of the magnetic field for the fixed value of the single-ion anisotropy $D/J = 0.05$ and four selected temperatures.

V. SPIN SQUEEZING

A complementary investigation of quantum properties of the mixed spin-(1/2,1,1/2) Heisenberg trimer involves

the spin squeezing, which can be quantified through the spin squeezing parameter whose definition is based on the uncertainty of spin measurements along different spatial directions. This measure quantifies the degree to which

quantum correlations within a multi-particle spin state reduce the variance of a specific spin component [38]:

$$\xi^2 = \frac{2(\Delta\hat{\mathcal{J}}_{\vec{n}_\perp})^2}{|\langle\hat{\mathcal{J}}\rangle|}, \quad (14)$$

where $\hat{\mathcal{J}} = \hat{\mathbf{s}}_a + \hat{\mathbf{S}}_b + \hat{\mathbf{s}}_c$ is the sum of spin operators. For our mixed spin model, we consider the maximum total number of spins as $L' = 4$ where $|\langle\hat{\mathcal{J}}\rangle| = L'/2$. This originates from the effective four spin-1/2 system by assuming a spin-1 particle as two interacting spin-1/2 particles. Keeping this assumption in mind, and considering the mean spin along the z -direction, \vec{n}_\perp will align in the x - y plane: $\hat{\mathcal{J}}_{\vec{n}_\perp} = \cos\theta\hat{\mathcal{J}}_x + \sin\theta\hat{\mathcal{J}}_y$, with the variance

$$\begin{aligned} (\Delta\hat{\mathcal{J}}_{\vec{n}_\perp})^2 &= \langle\hat{\mathcal{J}}_{\vec{n}_\perp}^2\rangle - \langle\hat{\mathcal{J}}_{\vec{n}_\perp}\rangle^2 \\ &= \langle\hat{\mathcal{J}}_x^2 + \hat{\mathcal{J}}_y^2\rangle + \cos(2\theta)\langle\hat{\mathcal{J}}_x^2 - \hat{\mathcal{J}}_y^2\rangle \\ &\quad + \sin(2\theta)\langle\hat{\mathcal{J}}_x\hat{\mathcal{J}}_y + \hat{\mathcal{J}}_y\hat{\mathcal{J}}_x\rangle. \end{aligned} \quad (15)$$

Consequently, the spin squeezing parameter is calculated by minimizing the variance with respect to θ . Note that $\langle\hat{\mathcal{J}}_\alpha\rangle = \langle\hat{\mathcal{J}}_\alpha\hat{\mathcal{J}}_z\rangle = \langle\hat{\mathcal{J}}_z\hat{\mathcal{J}}_\alpha\rangle = 0$, $\alpha \in \{x, y\}$. After a straightforward manipulation the spin squeezing parameter becomes [38]:

$$\xi^2 = \frac{2}{L'} \left[\langle\hat{\mathcal{J}}_x^2 + \hat{\mathcal{J}}_y^2\rangle - \sqrt{\langle\hat{\mathcal{J}}_x^2 - \hat{\mathcal{J}}_y^2\rangle^2 + \langle[\hat{\mathcal{J}}_x, \hat{\mathcal{J}}_y]_+\rangle^2} \right], \quad (16)$$

where $[\hat{\mathcal{J}}_x, \hat{\mathcal{J}}_y]_+ = \hat{\mathcal{J}}_x\hat{\mathcal{J}}_y + \hat{\mathcal{J}}_y\hat{\mathcal{J}}_x$ is the anticommutator for operators $\hat{\mathcal{J}}_x$ and $\hat{\mathcal{J}}_y$. To bring insight into the spin squeezing of the mixed spin-(1/2,1,1/2) Heisenberg trimeric cluster, the spin squeezing parameter was calculated according to Eq. (16) in a thermal state $\hat{\rho}$ as a function of the magnetic field $g\mu_B B/J$ at a few selected temperatures and a fixed value of the single-ion anisotropy $D/J = 0.05$. Fig. 4(a) bears evidence that the ground state of the mixed spin-(1/2,1,1/2) Heisenberg trimer can be either a squeezed, unsqueezed or a coherent state. The triplet ground state emerging at moderate magnetic fields $g\mu_B B/J > 1$ belongs to a coherent state with $\xi^2 = 1$, whereas the singlet ground state emerging at lower fields $g\mu_B B/J < 1$ features a spin squeezing $\xi^2 < 1$ (see black curve for $k_B T/J = 0.002$). It is also evidence that close to the critical magnetic field $g\mu_B B/J = 1$, the state of the system becomes unsqueezed ($\xi^2 > 1$). With increase of the temperature, the state of the system remains squeezed for higher magnetic fields. The inset of Fig. 4(a) actually verifies the behavior of ξ^2 as a function of the magnetic field at sufficiently low temperature $k_B T/J = 0.1$. It is evident from the inset that the system is indeed in a squeezed state $\xi^2 < 1$ at low enough magnetic fields $g\mu_B B/J \lesssim 1$, while it is evolving to an unsqueezed state $\xi^2 = 1$ at higher magnetic fields $g\mu_B B/J \gtrsim 1$. With a further increase of the magnetic field, the state of the system becomes coherent.

This illustrates how the applied magnetic field can significantly influence the nature of the state of a quantum system at low temperature.

In Fig. 4(b), we illustrate temperature variations of the spin squeezing parameter ξ^2 for the mixed spin-(1/2,1,1/2) Heisenberg trimer at six different values of the magnetic field. As the magnetic field increases, the temperature at which the largest spin squeezing is achieved (i.e. the smallest ξ^2) shifts to higher values. This indicates that lower magnetic fields stabilize the squeezed state, which consequently allows a more significant spin squeezing at higher temperatures. Interestingly, for the critical magnetic field $g\mu_B B/J = 1$ (blue solid line in Fig. 4(b)), the behavior of the squeezing parameter is quite different. It reaches its maximum at finite low temperatures and then gradually decreases with increasing temperature. From this figure, it can be seen that for fields below the critical value $g\mu_B B/J = 1$, the squeezing parameter shows a global minimum, while for higher fields $g\mu_B B/J > 1$, it exhibits a smooth decrease upon heating. Eventually, this parameter tends to the value $\xi^2 = 5/6$ at high temperatures that is the indication of the thermal steady-squeezed state.

Figure 4(c) displays a density plot of the spin squeezing parameter ξ^2 across $g\mu_B B/J - k_B T/J$ plane. The color scale at the top indicates values of the spin squeezing parameter ξ^2 ranging from 0.508 to 1.5. At lower magnetic fields than the critical value $g\mu_B B/J = 1$, the system can achieve a global minimum ξ_{\min}^2 . The line of yellow circles illustrates positions of this global minimum ξ_{\min}^2 in the $g\mu_B B/J - k_B T/J$ plane. At low magnetic fields, ξ_{\min}^2 is found at lower temperatures indicating significant spin squeezing in this regime. As the magnetic field increases, the position of ξ_{\min}^2 shifts towards higher temperatures. This shift suggests that stronger magnetic fields are needed to maintain the global minimum of spin squeezing at higher temperatures. This behavior indicates the intricate interplay between thermal fluctuations and the applied magnetic field in the degree of the squeezing parameter. To summarize, it has been verified that the mixed spin-(1/2,1,1/2) Heisenberg trimer can be driven from a coherent state to a spin squeezed state and hence, it has potential application in quantum information processing and quantum sensing where the enhancement of spin squeezing is crucial.

Next, let us examine the impact of the applied magnetic field on a spin squeezing state within the mixed spin-(1/2,1,1/2) Heisenberg trimer by utilizing a quasi-probability distribution based on the Husimi Q -function. The Husimi Q -function is mathematically defined as:

$$Q(\theta, \phi) = \frac{1}{\pi} \langle\alpha|\hat{\rho}|\alpha\rangle, \quad (17)$$

where $\hat{\rho}$ (5) represents the density operator of the system. The vector $|\alpha\rangle$ corresponds to a spin coherent state unambiguously given by spherical coordinates θ and ϕ on the Bloch sphere combining these two spherical angles

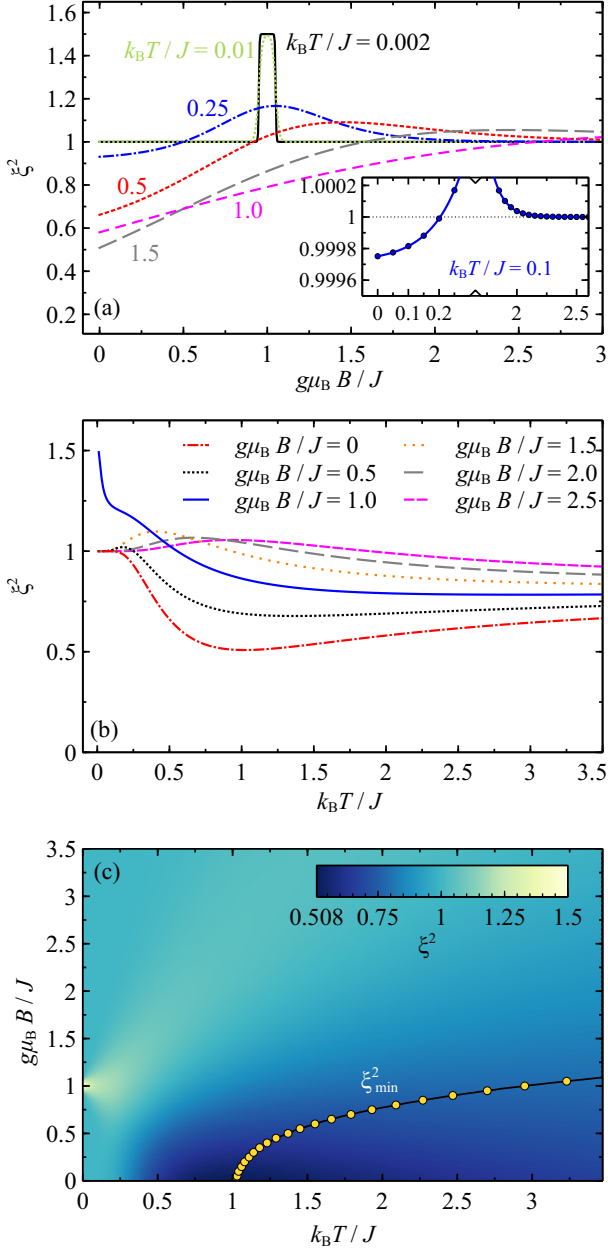


FIG. 4. (a) The spin squeezing parameter (16) of the mixed spin-(1/2,1,1/2) Heisenberg trimer as a function of the magnetic field at several different temperatures. The inset shows a detail for the parameter space at low enough temperature $k_B T/J = 0.1$. (b) Temperature variations of the spin squeezing parameter ξ^2 for several values of the magnetic field. (c) The density plot the squeezing parameter in the $g\mu_B B/J - k_B T/J$ plane. The line marked with yellow circles indicates the position of global minimum squeezing ξ_{\min}^2 in the $g\mu_B B/J - k_B T/J$ plane. The light region indicates that the state of the system becomes unsqueezed where the squeezing parameter reaches its maximum 1.5 close to the critical magnetic field $g\mu_B B/J = 1$ at low temperature. In all panels, a fixed value of the single-ion anisotropy $D/J = 0.05$ was assumed.

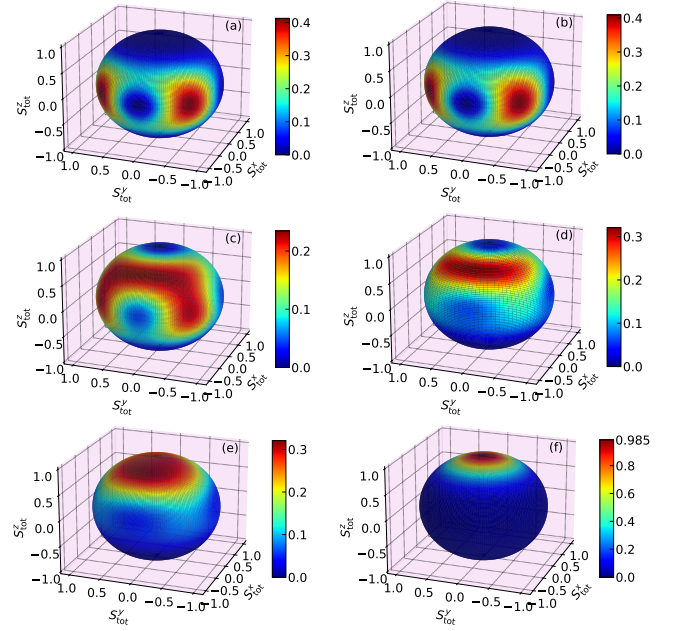


FIG. 5. The Husimi Q -function calculated for a thermal state of the mixed spin-(1/2,1,1/2) Heisenberg trimer characterized through the density operator ρ (5) at a fixed value of temperature $k_B T/J = 0.1$, the single-ion anisotropy $D/J = 0.05$ and a few selected values of the magnetic field: (a) $g\mu_B B/J = 0.0$, (b) $g\mu_B B/J = 0.5$, (c) $g\mu_B B/J = 1.0$, (d) $g\mu_B B/J = 1.5$, (e) $g\mu_B B/J = 2.0$, (f) $g\mu_B B/J = 2.5$.

into a single complex parameter:

$$\alpha = \sin \theta \cos \phi + i \sin \theta \sin \phi. \quad (18)$$

The spin coherent state $|\alpha\rangle$ is the state obtained by rotating the highest-weight \hat{S}_T^z eigenstate $|\uparrow 1 \uparrow\rangle$ counterclockwise by angle θ about the y -axis, and then by angle ϕ about the z -axis: $|\alpha\rangle = e^{i\phi\hat{J}_z} e^{i\theta\hat{J}_y} |\uparrow 1 \uparrow\rangle$. The coherent state $|\alpha\rangle$ can be also introduced in terms of the angular momentum raising and lowering operators $\hat{J}_{\pm} = \hat{J}_x \pm i\hat{J}_y$ as follows:

$$|\alpha\rangle = \exp\left[\frac{\theta}{2}\left(\hat{J}_- e^{i\phi} - \hat{J}_+ e^{-i\phi}\right)\right] |\uparrow 1 \uparrow\rangle. \quad (19)$$

We have implemented QuTiP toolbox [65, 66] for calculating the Husimi Q -function for the mixed spin-(1/2,1,1/2) Heisenberg trimer at a fixed value of temperature $k_B T/J = 0.1$, the single-ion anisotropy $D/J = 0.05$ and a few selected values of the magnetic field, which provides additional insight into the squeezing effect particularly illuminated in the inset of Fig. 4(a). In the squeezed region $g\mu_B B/J < 1$ with $\xi^2 < 1$, this operation produces a squeezed state that is stretched both along x - and y -directions as illustrated in Figs. 5(a) and (b). In a vicinity of the transition field $g\mu_B B/J \approx 1$, the squeezing property starts to fade as exemplified by Fig. 5(c). Fig. 5(d)-(f) illustrates the Husimi Q -function for the unsqueezed parameter region $g\mu_B B/J > 1$, where the spin

squeezed state counterproductively diminishes. Therefore, the state is sufficiently squeezed only if a strength of the magnetic field is lower than the transition field $g\mu_B B_c/J \approx 1$. For instance, an unsqueezed kicked top displayed in Fig. 5(f) showcases a coherent state with a Gaussian distribution of quantum fluctuations, which results from a quasi-probability distribution with a circular cross-section whose probability density is highest at the center and gradually diminishes outwards.

VI. QUANTUM FEATURES OF MOLECULAR NANOMAGNET $\text{Cu}^{\text{II}}\text{Ni}^{\text{II}}\text{Cu}^{\text{II}}$

In this section, we present a theoretical prediction for the degree of tripartite entanglement, coherence, and spin squeezing parameter of the heterotrimeric molecular nanomagnet $\text{Cu}^{\text{II}}\text{Ni}^{\text{II}}\text{Cu}^{\text{II}}$, which represents an experimental realization of the mixed spin-(1/2,1,1/2) Heisenberg trimer. It has been verified in Ref. [57] that magnetic properties of the molecular compound $\text{Cu}^{\text{II}}\text{Ni}^{\text{II}}\text{Cu}^{\text{II}}$ can be accurately modeled by the mixed spin-(1/2,1,1/2) Heisenberg trimer with an isotropic exchange-coupling constant $J = 22.8 \text{ cm}^{-1}$, a small nonzero single-ion anisotropy $D = 0.05 \text{ cm}^{-1}$, and an average gyromagnetic ratio $g = 2.227$ for Cu^{2+} and Ni^{2+} magnetic ions [57]. We will use this set of parameters to make theoretical predictions for the tripartite negativity, coherence, and spin squeezing parameter of the heterotrimeric molecular complex $\text{Cu}^{\text{II}}\text{Ni}^{\text{II}}\text{Cu}^{\text{II}}$.

Fig. 6(a) illustrates temperature dependencies of the tripartite negativity N_{abc} of the mixed spin-(1/2,1,1/2) Heisenberg trimer adjusted to a theoretical modeling of the molecular nanomagnet $\text{Cu}^{\text{II}}\text{Ni}^{\text{II}}\text{Cu}^{\text{II}}$ for several values of the magnetic field. At zero magnetic field, the tripartite negativity gradually decreases upon increasing temperature when starting from a zero-temperature asymptotic limit $N_{\text{abc}} = 5/8$ and vanishing approximately at the threshold temperature $T \approx 37 \text{ K}$. The same general trends can be also detected at magnetic fields below critical value $B = J$ (black line marked with circles) favoring the singlet ground state $|\psi_9\rangle$. In the range of magnetic fields between special points $B = J$ and $B = 2J$ (blue line marked with hexagons), the tripartite negativity starts from a lower local maximum of around $N_{\text{abc}} \approx 0.454$. The weaker value of the tripartite entanglement bears a close relation with presence of the triplet ground state $|\psi_5\rangle$, but the respective threshold temperature remains unaffected by this change. A notable non-monotonous thermal dependence of the tripartite negativity is finally observed when the magnetic field slightly exceeds the saturation value $B \approx 2J$. Under such conditions, the tripartite negativity N_{abc} exhibits a reentrant behavior when it first becomes nonzero at a lower threshold temperature, then rises steadily to a relatively low local maximum, which is successively followed by a gradual monotonous decline until it completely disappears at a higher threshold temperature (see the par-

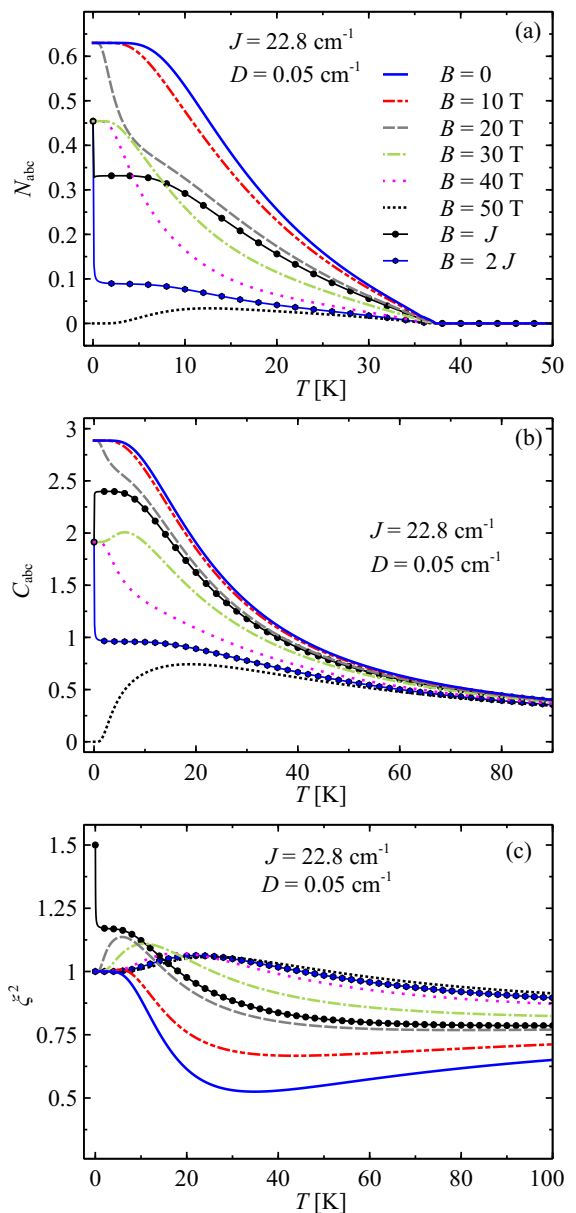


FIG. 6. Temperature variations of three basic quantum characteristics of the mixed spin-(1/2,1,1/2) Heisenberg trimer with an exchange-coupling constant $J = 22.8 \text{ cm}^{-1}$, a single-ion anisotropy $D = 0.05 \text{ cm}^{-1}$, and gyromagnetic ratio $g = 2.227$ adjusted according to Ref. [57] to a theoretical modeling of the molecular nanomagnet $\text{Cu}^{\text{II}}\text{Ni}^{\text{II}}\text{Cu}^{\text{II}}$ at a few different magnetic field strengths: (a) the tripartite negativity N_{abc} , (b) the quantum coherence C_{abc} , (c) the spin squeezing parameter ξ^2 . The labels for the magnetic field is given in the panel (a).

ticular case for $B = 50 \text{ T}$).

Fig. 6(b) displays typical temperature dependencies of the quantum coherence C_{abc} of the mixed spin-(1/2,1,1/2) Heisenberg trimer by adapting the same set

of parameters as used in Fig. 6(a) for a theoretical modeling of the tripartite entanglement of the molecular complex $\text{Cu}^{\text{II}}\text{Ni}^{\text{II}}\text{Cu}^{\text{II}}$. At low temperatures, the coherence C_{abc} exhibits a quite analogous behavior to the tripartite negativity including three different zero-temperature asymptotic values assigned to the singlet ground state $|\psi_9\rangle$, the triplet ground state $|\psi_5\rangle$, and the fully polarized ground state $|\psi_{11}\rangle$, respectively. In contrast to the tripartite negativity, the coherence C_{abc} does not completely vanish at the threshold temperature but it persists of being nonzero in a high-temperature regime due to a more gradual thermally-induced decay. This observation bears evidence that the molecular nanomagnet $\text{Cu}^{\text{II}}\text{Ni}^{\text{II}}\text{Cu}^{\text{II}}$ retains a certain degree of quantum coherence even at elevated temperatures, which are well above the threshold temperature where the quantum entanglement is completely lost.

Last but not least, Fig. 6(c) illustrates typical temperature variations of the spin squeezing parameter ξ^2 calculated from Eq. (16) specifically for the mixed spin-(1/2,1,1/2) Heisenberg trimer resembling the molecular complex $\text{Cu}^{\text{II}}\text{Ni}^{\text{II}}\text{Cu}^{\text{II}}$. The spin squeezing parameter ξ^2 allows to distinguish a coherent spin state from a squeezed one. For nonzero magnetic field with excluding critical point $B = J$ (black line marked with circles), at low enough temperatures, the spin squeezing parameter approaches the value $\xi^2 = 1$ indicating a perfect coherent state. With raising the temperature, this parameter starts to increase and reaches a round maximum then gradually decreases until surpasses the coherent limit. At zero magnetic field (blue line), the spin squeezing parameter ξ^2 drops down upon increasing temperature to a global minimum observed around $T \approx 30$ K. This global minimum becomes gradually flattens and shifts towards higher temperatures as the magnetic field strengthens. After reaching the global minimum, the squeezing parameter ξ^2 rises steadily with temperature that suggests a reduction in quantum correlations and entanglement. The increase in the spin squeezing parameter ξ^2 continues up to a certain temperature, beyond which it tends to $\xi^2 \approx 5/6$ where a the state of the system is steady-state spin squeezed. As discussed in Fig. 4(b), for the special case $B = J$ we see that the parameter ξ^2 is in its maximum value 1.5 at $T \approx 0$. Then with increase of the temperature, it decreases and surpasses the coherent limit near the temperature $T \approx 20$ K and reaches constant value $\xi^2 \approx 0.75$ at sufficiently high temperature.

The observed behavior of the spin squeezing parameter can be related to the previously discussed tripartite entanglement and quantum coherence. At low temperatures, the initial drop in the the spin squeezing parameter ξ^2 corresponds to the presence of tripartite entanglement with still sizable quantum correlations at the global minimum. On the other hand, the nonmonotonic behavior of the tripartite negativity N_{abc} observed at sufficiently high magnetic fields $B \gtrsim 2J$ T, where the negativity first increases before ultimately declining, may also be reflected in a gradual decrease of the spin squeezing pa-

rameter ξ^2 without reaching a global minimum under similar conditions (see black dotted lines in Fig. 6(a) and 6(c) for $B = 50$ T). Although the spin squeezing parameter ξ^2 increases with temperature in a high-temperature regime it never approaches the maximal value $\xi^2 = 1$ what signifies a loss of quantum coherence due to the thermal decoherence.

VII. CONCLUSIONS

In the present paper, we have comprehensively investigated basic quantum characteristics of the mixed spin-(1/2,1,1/2) Heisenberg trimer in a presence of the external magnetic field, which was designed for a theoretical modeling of molecular nanomagnets such as the heterotrimeric coordination compound $\text{Cu}^{\text{II}}\text{Ni}^{\text{II}}\text{Cu}^{\text{II}}$. By employing rigorous analytical and numerical calculations, we have examined distributions of bipartite and tripartite entanglement, the l_1 -norm of quantum coherence, and the spin squeezing parameter under the influence of an external magnetic field. The key finding stemming from the present study is that the mixed spin-(1/2,1,1/2) Heisenberg trimer may display significant bipartite and tripartite entanglement up to relatively high temperatures and magnetic fields, whereby the quantum coherence is maintained even at elevated temperatures compared to entanglement. This indicates that the investigated quantum spin system may retain a high degree of the quantum coherence despite strong thermal fluctuations. As far as the spin squeezing is concerned, the temperature at which the largest spin squeezing is achieved shifts to higher values upon strengthening of the magnetic field. This result implies that smaller magnetic fields stabilize the squeezed state and allow more significant spin squeezing at lower temperatures. The intricate interplay between quantum fluctuations and thermal effects is crucial for optimizing conditions for achieving maximal spin squeezing, which is vital for applications in quantum information processing and quantum sensing.

Exact results for quantum features of the mixed spin-(1/2,1,1/2) Heisenberg trimer has been also adapted for a theoretical modeling of the heterotrimeric molecular nanomagnet $\text{Cu}^{\text{II}}\text{Ni}^{\text{II}}\text{Cu}^{\text{II}}$. It has been verified that the molecular complex $\text{Cu}^{\text{II}}\text{Ni}^{\text{II}}\text{Cu}^{\text{II}}$ exhibits a significant bipartite entanglement between $\text{Cu}^{\text{II}}\text{-Ni}^{\text{II}}$ magnetic ions and a significant tripartite entanglement between $\text{Cu}^{\text{II}}\text{-Ni}^{\text{II}}\text{-Cu}^{\text{II}}$ magnetic ions, which persist up to relatively high temperatures 37 K and magnetic fields 50 T. In addition, it has been theoretically predicted that molecular nanomagnet $\text{Cu}^{\text{II}}\text{Ni}^{\text{II}}\text{Cu}^{\text{II}}$ displays a high degree of the quantum coherence persisting even at elevated temperatures in spite of strong thermal fluctuations. Last but not least, our theoretical results for the molecular compound $\text{Cu}^{\text{II}}\text{Ni}^{\text{II}}\text{Cu}^{\text{II}}$ also reveal optimal conditions for achieving the highest degree of the spin squeezing, which are achieved at zero magnetic field around $T \approx 20$ K corresponding to the global minimum of the spin squeezing pa-

TABLE I. Eigenvectors, total quantum spin number S_T^z , and eigenenergies of the mixed spin-(1/2,1,1/2) Heisenberg trimer.

Eigenvectors	S_T^z	Eigenenergies
$ \psi_1\rangle = \frac{1}{\sqrt{2}}(\downarrow 0 \uparrow\rangle - \uparrow 0 \downarrow\rangle)$	0	$E_1 = 0$
$ \psi_2\rangle = \frac{1}{\sqrt{2}}(\downarrow 1 \downarrow\rangle - \uparrow -1 \uparrow\rangle)$	0	$E_2 = D - J$
$ \psi_3\rangle = \frac{1}{\sqrt{2}}(\downarrow 1 \uparrow\rangle - \uparrow 1 \downarrow\rangle)$	1	$E_3 = D - h$
$ \psi_4\rangle = \frac{1}{\sqrt{2}}(\downarrow -1 \uparrow\rangle - \uparrow -1 \downarrow\rangle)$	-1	$E_4 = D + h$
$ \psi_5\rangle = a(\uparrow 1 \downarrow\rangle + \downarrow 1 \uparrow\rangle) + b \uparrow 0 \uparrow\rangle$	1	$E_5 = \frac{D}{2} - h - \frac{1}{2}\sqrt{D^2 + 4J^2}$
$ \psi_6\rangle = c(\uparrow 1 \downarrow\rangle + \downarrow 1 \uparrow\rangle) + d \uparrow 0 \uparrow\rangle$	1	$E_6 = \frac{D}{2} - h + \frac{1}{2}\sqrt{D^2 + 4J^2}$
$ \psi_7\rangle = a(\uparrow -1 \downarrow\rangle + \downarrow -1 \uparrow\rangle) + b \downarrow 0 \downarrow\rangle$	-1	$E_7 = \frac{D}{2} + h - \frac{1}{2}\sqrt{D^2 + 4J^2}$
$ \psi_8\rangle = c(\uparrow -1 \downarrow\rangle + \downarrow -1 \uparrow\rangle) + d \downarrow 0 \downarrow\rangle$	-1	$E_8 = \frac{D}{2} + h + \frac{1}{2}\sqrt{D^2 + 4J^2}$
$ \psi_9\rangle = e(\uparrow 0 \downarrow\rangle + \downarrow 0 \uparrow\rangle) + f(\uparrow -1 \uparrow\rangle + \downarrow 1 \downarrow\rangle)$	0	$E_9 = \frac{D-J}{2} - \sqrt{(\frac{D-J}{2})^2 + 2J^2}$
$ \psi_{10}\rangle = g(\uparrow 0 \downarrow\rangle + \downarrow 0 \uparrow\rangle) + h(\uparrow -1 \uparrow\rangle + \downarrow 1 \downarrow\rangle)$	0	$E_{10} = \frac{D-J}{2} + \sqrt{(\frac{D-J}{2})^2 + 2J^2}$
$ \psi_{11}\rangle = \uparrow \uparrow \uparrow\rangle$	2	$E_{11} = D + J - 2h$
$ \psi_{12}\rangle = \downarrow -1 \downarrow\rangle$	-2	$E_{12} = D + J + 2h$

TABLE II. Probability amplitudes of the eigenvectors of the mixed spin-(1/2,1,1/2) Heisenberg trimer.

$a = \frac{\frac{D}{2} - \sqrt{J^2 + (\frac{D}{2})^2}}{\sqrt{2J^2 + 2\left(\frac{D}{2} - \sqrt{J^2 + (\frac{D}{2})^2}\right)^2}}$	$b = \frac{J}{\sqrt{J^2 + \left(\frac{D}{2} - \sqrt{J^2 + (\frac{D}{2})^2}\right)^2}}$
$c = \frac{\frac{D}{2} + \sqrt{J^2 + (\frac{D}{2})^2}}{\sqrt{2J^2 + 2\left(\frac{D}{2} + \sqrt{J^2 + (\frac{D}{2})^2}\right)^2}}$	$d = \frac{J}{\sqrt{J^2 + \left(\frac{D}{2} + \sqrt{J^2 + (\frac{D}{2})^2}\right)^2}}$
$e = \frac{J}{\sqrt{2J^2 + \left(\frac{D-J}{2} - \sqrt{2J^2 + (\frac{D-J}{2})^2}\right)^2}}$	$f = \frac{\frac{D-J}{2} - \sqrt{2J^2 + (\frac{D-J}{2})^2}}{\sqrt{4J^2 + 2\left(\frac{D-J}{2} - \sqrt{2J^2 + (\frac{D-J}{2})^2}\right)^2}}$
$g = \frac{J}{\sqrt{2J^2 + \left(\frac{D-J}{2} + \sqrt{2J^2 + (\frac{D-J}{2})^2}\right)^2}}$	$h = \frac{\frac{D-J}{2} + \sqrt{2J^2 + (\frac{D-J}{2})^2}}{\sqrt{4J^2 + 2\left(\frac{D-J}{2} + \sqrt{2J^2 + (\frac{D-J}{2})^2}\right)^2}}$

parameter. To summarize, our analysis underscores the importance of the magnetic field and temperature in modulating the bipartite and tripartite entanglement, quantum coherence, and spin squeezing in molecular nanomagnet $\text{Cu}^{\text{II}}\text{Ni}^{\text{II}}\text{Cu}^{\text{II}}$ and related group of magnetic materials, which pave the way for advanced applications in quantum technologies

ACKNOWLEDGEMENTS

A.G. acknowledges Saeed's Quantum Information Group (SSQIG) for accommodating hospitality during

the course of this project. H.A.Z. acknowledges the financial support provided under the postdoctoral fellowship program of P. J. Šafárik University in Košice, Slovakia. S.H. was supported by Semnan University under Contract No. 21270. J.S. acknowledges financial support by the grant of Slovak Research and Development Agency provided under the contract No. APVV-22-0172 and by the grant of The Ministry of Education, Research, Development and Youth of the Slovak Republic under the contract No. VEGA 1/0695/23. V.O and Zh. A. acknowledge partial financial support from ANSEF (Grant No. PS-condmatth-2884) and from CS RA MESCO (Grants No. 21AG-1C047, 21AG-1C006 and 23AA-1C032).

Appendix A: Eigenvectors and eigenenergies

Eigenvectors of the mixed spin-(1/2,1,1/2) Heisenberg trimer given by the Hamiltonian 1 are defined in Table I, whereby the respective probability amplitudes entering into the relevant eigenvectors are specifically given in Table II. with the corresponding probability amplitudes given in Table II.

Appendix B: The total, partially transposed and reduced density matrices

The total density matrix ρ of the mixed spin-(1/2,1,1/2) Heisenberg trimer reads:

$$\rho = \begin{pmatrix} \rho_{1,1} & 0 & 0 & 0 & 0 & 0 & 0 & 0 & 0 & 0 & 0 & 0 \\ 0 & \rho_{2,2} & \rho_{2,3} & 0 & 0 & 0 & \rho_{2,7} & 0 & 0 & 0 & 0 & 0 \\ 0 & \rho_{2,3} & \rho_{3,3} & 0 & 0 & 0 & \rho_{3,7} & 0 & 0 & 0 & 0 & 0 \\ 0 & 0 & 0 & \rho_{4,4} & \rho_{4,5} & 0 & 0 & \rho_{4,8} & \rho_{4,9} & 0 & 0 & 0 \\ 0 & 0 & 0 & \rho_{4,5} & \rho_{5,5} & 0 & 0 & \rho_{5,8} & \rho_{5,9} & 0 & 0 & 0 \\ 0 & 0 & 0 & 0 & 0 & \rho_{6,6} & 0 & 0 & 0 & \rho_{6,10} & \rho_{6,11} & 0 \\ 0 & \rho_{2,7} & \rho_{3,7} & 0 & 0 & 0 & \rho_{7,7} & 0 & 0 & 0 & 0 & 0 \\ 0 & 0 & 0 & \rho_{4,8} & \rho_{5,8} & 0 & 0 & \rho_{8,8} & \rho_{8,9} & 0 & 0 & 0 \\ 0 & 0 & 0 & \rho_{4,9} & \rho_{5,9} & 0 & 0 & \rho_{8,9} & \rho_{9,9} & 0 & 0 & 0 \\ 0 & 0 & 0 & 0 & 0 & \rho_{6,10} & 0 & 0 & 0 & \rho_{10,10} & \rho_{10,11} & 0 \\ 0 & 0 & 0 & 0 & 0 & \rho_{6,11} & 0 & 0 & 0 & \rho_{10,11} & \rho_{11,11} & 0 \\ 0 & 0 & 0 & 0 & 0 & 0 & 0 & 0 & 0 & 0 & 0 & \rho_{12,12} \end{pmatrix}$$

The partially transposed density matrices with respect to each spin s_a , S_b and s_c are denoted by ρ^{T_a} , ρ^{T_b} and ρ^{T_c} , given by:

$$\rho^{T_a} = \begin{pmatrix} \rho_{1,1} & 0 & 0 & 0 & 0 & 0 & 0 & \rho_{2,7} & \rho_{3,7} & 0 & 0 & 0 \\ 0 & \rho_{2,2} & \rho_{2,3} & 0 & 0 & 0 & 0 & 0 & 0 & \rho_{4,8} & \rho_{5,8} & 0 \\ 0 & \rho_{2,3} & \rho_{3,3} & 0 & 0 & 0 & 0 & 0 & 0 & \rho_{4,9} & \rho_{5,9} & 0 \\ 0 & 0 & 0 & \rho_{4,4} & \rho_{4,5} & 0 & 0 & 0 & 0 & 0 & 0 & \rho_{6,10} \\ 0 & 0 & 0 & \rho_{4,5} & \rho_{5,5} & 0 & 0 & 0 & 0 & 0 & 0 & \rho_{6,11} \\ 0 & 0 & 0 & 0 & 0 & \rho_{6,6} & 0 & 0 & 0 & 0 & 0 & 0 \\ 0 & 0 & 0 & 0 & 0 & 0 & \rho_{7,7} & 0 & 0 & 0 & 0 & 0 \\ \rho_{2,7} & 0 & 0 & 0 & 0 & 0 & 0 & \rho_{8,8} & \rho_{8,9} & 0 & 0 & 0 \\ \rho_{3,7} & 0 & 0 & 0 & 0 & 0 & 0 & \rho_{8,9} & \rho_{9,9} & 0 & 0 & 0 \\ 0 & \rho_{4,8} & \rho_{4,9} & 0 & 0 & 0 & 0 & 0 & 0 & \rho_{10,10} & \rho_{10,11} & 0 \\ 0 & \rho_{5,8} & \rho_{5,9} & 0 & 0 & 0 & 0 & 0 & 0 & \rho_{10,11} & \rho_{11,11} & 0 \\ 0 & 0 & 0 & \rho_{6,10} & \rho_{6,11} & 0 & 0 & 0 & 0 & 0 & 0 & \rho_{12,12} \end{pmatrix}$$

$$\rho^{T_b} = \begin{pmatrix} \rho_{1,1} & 0 & 0 & \rho_{2,3} & 0 & 0 & 0 & 0 & \rho_{3,7} & 0 & 0 & \rho_{5,8} \\ 0 & \rho_{2,2} & 0 & 0 & 0 & 0 & \rho_{2,7} & 0 & 0 & \rho_{4,8} & 0 & 0 \\ 0 & 0 & \rho_{3,3} & 0 & 0 & \rho_{4,5} & 0 & 0 & 0 & 0 & \rho_{5,9} & 0 \\ \rho_{2,3} & 0 & 0 & \rho_{4,4} & 0 & 0 & 0 & 0 & \rho_{4,9} & 0 & 0 & \rho_{6,10} \\ 0 & 0 & 0 & 0 & \rho_{5,5} & 0 & 0 & 0 & 0 & 0 & 0 & 0 \\ 0 & 0 & \rho_{4,5} & 0 & 0 & \rho_{6,6} & 0 & 0 & 0 & 0 & \rho_{6,11} & 0 \\ 0 & \rho_{2,7} & 0 & 0 & 0 & 0 & \rho_{7,7} & 0 & 0 & \rho_{8,9} & 0 & 0 \\ 0 & 0 & 0 & 0 & 0 & 0 & 0 & \rho_{8,8} & 0 & 0 & 0 & 0 \\ \rho_{3,7} & 0 & 0 & \rho_{4,9} & 0 & 0 & 0 & 0 & \rho_{9,9} & 0 & 0 & \rho_{10,11} \\ 0 & \rho_{4,8} & 0 & 0 & 0 & 0 & \rho_{8,9} & 0 & 0 & \rho_{10,10} & 0 & 0 \\ 0 & 0 & \rho_{5,9} & 0 & 0 & \rho_{6,11} & 0 & 0 & 0 & 0 & \rho_{11,11} & 0 \\ \rho_{5,8} & 0 & 0 & \rho_{6,10} & 0 & 0 & 0 & 0 & \rho_{10,11} & 0 & 0 & \rho_{12,12} \end{pmatrix}$$

$$\rho^{T_c} = \begin{pmatrix} \rho_{1,1} & 0 & 0 & \rho_{2,3} & 0 & 0 & 0 & \rho_{2,7} & 0 & 0 & 0 & 0 \\ 0 & \rho_{2,2} & 0 & 0 & 0 & 0 & 0 & 0 & 0 & 0 & 0 & 0 \\ 0 & 0 & \rho_{3,3} & 0 & 0 & \rho_{4,5} & \rho_{3,7} & 0 & 0 & \rho_{4,9} & 0 & 0 \\ \rho_{2,3} & 0 & 0 & \rho_{4,4} & 0 & 0 & 0 & \rho_{4,8} & 0 & 0 & 0 & 0 \\ 0 & 0 & 0 & 0 & \rho_{5,5} & 0 & 0 & 0 & \rho_{5,9} & 0 & 0 & \rho_{6,11} \\ 0 & 0 & \rho_{4,5} & 0 & 0 & \rho_{6,6} & \rho_{5,8} & 0 & 0 & \rho_{6,10} & 0 & 0 \\ 0 & 0 & \rho_{3,7} & 0 & 0 & \rho_{5,8} & \rho_{7,7} & 0 & 0 & \rho_{8,9} & 0 & 0 \\ \rho_{2,7} & 0 & 0 & \rho_{4,8} & 0 & 0 & 0 & \rho_{8,8} & 0 & 0 & 0 & 0 \\ 0 & 0 & 0 & 0 & \rho_{5,9} & 0 & 0 & 0 & \rho_{9,9} & 0 & 0 & \rho_{10,11} \\ 0 & 0 & \rho_{4,9} & 0 & 0 & \rho_{6,10} & \rho_{8,9} & 0 & 0 & \rho_{10,10} & 0 & 0 \\ 0 & 0 & 0 & 0 & 0 & 0 & 0 & 0 & 0 & 0 & \rho_{11,11} & 0 \\ 0 & 0 & 0 & 0 & \rho_{6,11} & 0 & 0 & 0 & \rho_{10,11} & 0 & 0 & \rho_{12,12} \end{pmatrix}$$

The reduced density matrix ϱ_{ab} is given by:

$$\varrho_{ab} = \begin{pmatrix} \rho_{1,1} + \rho_{2,2} & 0 & 0 & 0 & 0 & 0 \\ 0 & \rho_{3,3} + \rho_{4,4} & 0 & \rho_{2,3} + \rho_{4,5} & 0 & 0 \\ 0 & 0 & \rho_{5,5} + \rho_{6,6} & 0 & \rho_{4,5} + \rho_{6,10} & 0 \\ 0 & \rho_{2,3} + \rho_{4,5} & 0 & \rho_{7,7} + \rho_{8,8} & 0 & 0 \\ 0 & 0 & \rho_{4,5} + \rho_{6,10} & 0 & \rho_{9,9} + \rho_{10,10} & 0 \\ 0 & 0 & 0 & 0 & 0 & \rho_{11,11} + \rho_{12,12} \end{pmatrix}.$$

The partially transposed reduced density matrix $\varrho_{ab}^{\text{T}_b}$ is as follows:

$$\varrho_{ab}^{\text{T}_b} = \begin{pmatrix} \rho_{1,1} + \rho_{2,2} & 0 & 0 & 0 & \rho_{2,3} + \rho_{4,5} & 0 \\ 0 & \rho_{3,3} + \rho_{4,4} & 0 & 0 & 0 & \rho_{4,5} + \rho_{6,10} \\ 0 & 0 & \rho_{5,5} + \rho_{6,6} & 0 & 0 & 0 \\ 0 & 0 & 0 & \rho_{7,7} + \rho_{8,8} & 0 & 0 \\ \rho_{2,3} + \rho_{4,5} & 0 & 0 & 0 & \rho_{9,9} + \rho_{10,10} & 0 \\ 0 & \rho_{4,5} + \rho_{6,10} & 0 & 0 & 0 & \rho_{11,11} + \rho_{12,12} \end{pmatrix}.$$

The reduced density matrix ϱ_{ab} is given by:

$$\varrho_{ab} = \begin{pmatrix} \rho_{1,1} + \rho_{7,7} & 0 & 0 & 0 & 0 & 0 \\ 0 & \rho_{2,2} + \rho_{8,8} & \rho_{2,3} + \rho_{4,5} & 0 & 0 & 0 \\ 0 & \rho_{2,3} + \rho_{8,9} & \rho_{3,3} + \rho_{9,9} & 0 & 0 & 0 \\ 0 & 0 & 0 & \rho_{4,4} + \rho_{10,10} & \rho_{4,5} + \rho_{10,11} & 0 \\ 0 & 0 & 0 & \rho_{4,5} + \rho_{10,11} & \rho_{5,5} + \rho_{11,11} & 0 \\ 0 & 0 & 0 & 0 & 0 & \rho_{6,6} + \rho_{12,12} \end{pmatrix}.$$

The partially transposed reduced density matrix $\varrho_{ab}^{\text{T}_b}$ is as follows:

$$\varrho_{ab}^{\text{T}_b} = \begin{pmatrix} \rho_{1,1} + \rho_{7,7} & 0 & 0 & \rho_{2,3} + \rho_{8,9} & 0 & 0 \\ 0 & \rho_{2,2} + \rho_{8,8} & 0 & 0 & 0 & 0 \\ 0 & 0 & \rho_{3,3} + \rho_{9,9} & 0 & 0 & \rho_{4,5} + \rho_{10,11} \\ \rho_{2,3} + \rho_{8,9} & 0 & 0 & \rho_{4,4} + \rho_{10,10} & 0 & 0 \\ 0 & 0 & 0 & 0 & \rho_{5,5} + \rho_{11,11} & 0 \\ 0 & 0 & \rho_{4,5} + \rho_{10,11} & 0 & 0 & \rho_{6,6} + \rho_{12,12} \end{pmatrix}.$$

The reduced density matrix ϱ_{ac} would be given by the following formula:

$$\varrho_{ac} = \begin{pmatrix} \rho_{1,1} + \rho_{3,3} + \rho_{5,5} & 0 & 0 & 0 \\ 0 & \rho_{2,2} + \rho_{4,4} + \rho_{6,6} & \rho_{2,7} + \rho_{4,9} + \rho_{6,11} & 0 \\ 0 & \rho_{2,7} + \rho_{4,9} + \rho_{6,11} & \rho_{7,7} + \rho_{9,9} + \rho_{11,11} & 0 \\ 0 & 0 & 0 & \rho_{8,8} + \rho_{10,10} + \rho_{12,12} \end{pmatrix}.$$

The partially transposed density matrix $\varrho_{ac}^{\text{T}_c}$ takes the form:

$$\varrho_{ac}^{\text{T}_a} = \begin{pmatrix} \rho_{1,1} + \rho_{3,3} + \rho_{5,5} & 0 & 0 & \rho_{2,7} + \rho_{4,9} + \rho_{6,11} \\ 0 & \rho_{2,2} + \rho_{4,4} + \rho_{6,6} & 0 & 0 \\ 0 & 0 & \rho_{7,7} + \rho_{9,9} + \rho_{11,11} & 0 \\ \rho_{2,7} + \rho_{4,9} + \rho_{6,11} & 0 & 0 & \rho_{8,8} + \rho_{10,10} + \rho_{12,12} \end{pmatrix}.$$

The elements of the density matrix are presented below where Z is the partition function given in formula (3):

$$\begin{aligned}
\rho_{1,1} &= \frac{1}{Z} \exp(-\beta E_{11}) \\
\rho_{2,2} &= \rho_{7,7} = \frac{1}{Z} \left[\frac{1}{2} \exp(-\beta E_3) + a^2 \exp(-\beta E_5) + c^2 \exp(-\beta E_6) \right] \\
\rho_{2,3} &= \rho_{3,7} = \frac{1}{Z} [ab \exp(-\beta E_5) + cd \exp(-\beta E_6)] \\
\rho_{2,7} &= \frac{1}{Z} \left[-\frac{1}{2} \exp(-\beta E_3) + a^2 \exp(-\beta E_5) + c^2 \exp(-\beta E_6) \right] \\
\rho_{3,3} &= \frac{1}{Z} [b^2 \exp(-\beta E_5) + d^2 \exp(-\beta E_6)] \\
\rho_{4,4} &= \rho_{99} = \frac{1}{Z} \left[\frac{1}{2} \exp(-\beta E_1) + e^2 \exp(-\beta E_9) + g^2 \exp(-\beta E_{10}) \right] \\
\rho_{4,5} &= \rho_{4,8} = \rho_{5,9} = \rho_{8,9} = \frac{1}{Z} [ef \exp(-\beta E_9) + gh \exp(-\beta E_{10})] \\
\rho_{4,9} &= \frac{1}{Z} \left[-\frac{1}{2} \exp(-\beta E_1) + e^2 \exp(-\beta E_9) + g^2 \exp(-\beta E_{10}) \right] \\
\rho_{5,5} &= \rho_{88} = \frac{1}{Z} \left[\frac{1}{2} \exp(-\beta E_2) + f^2 \exp(-\beta E_9) + h^2 \exp(-\beta E_{10}) \right] \\
\rho_{5,8} &= \frac{1}{Z} \left[-\frac{1}{2} \exp(-\beta E_2) + f^2 \exp(-\beta E_9) + h^2 \exp(-\beta E_{10}) \right] \\
\rho_{6,6} &= \rho_{11,11} = \frac{1}{Z} \left[\frac{1}{2} \exp(-\beta E_4) + a^2 \exp(-\beta E_7) + c^2 \exp(-\beta E_8) \right] \\
\rho_{6,10} &= \rho_{10,11} = \frac{1}{Z} [ab \exp(-\beta E_7) + cd \exp(-\beta E_8)] \\
\rho_{6,11} &= \frac{1}{Z} \left[-\frac{1}{2} \exp(-\beta E_4) + a^2 \exp(-\beta E_7) + c^2 \exp(-\beta E_8) \right] \\
\rho_{10,10} &= \frac{1}{Z} [b^2 \exp(-\beta E_7) + d^2 \exp(-\beta E_8)] \\
\rho_{12,12} &= \frac{1}{Z} \exp(-\beta E_{12})
\end{aligned}$$

All eigenvalues of the partially transposed reduced density matrix $\rho_{ab}^{\text{T}_b}$ that constitute bipartite negativity N_{ab} (according to the formula) are as follows:

$$\lambda_1 = \rho_{2,2} + \rho_{8,8}, \quad \lambda_2 = \rho_{5,5} + \rho_{11,11},$$

$$\lambda_{3;4} = \frac{1}{2} \left(\rho_{1,1} + \rho_{7,7} + \rho_{4,4} + \rho_{10,10} \pm \sqrt{(\rho_{1,1} + \rho_{7,7} - \rho_{4,4} - \rho_{10,10})^2 + 4(\rho_{2,3} + \rho_{8,9})^2} \right),$$

and

$$\lambda_{5;6} = \frac{1}{2} \left(\rho_{3,3} + \rho_{9,9} + \rho_{6,6} + \rho_{12,12} \pm \sqrt{(\rho_{3,3} + \rho_{9,9} - \rho_{6,6} - \rho_{12,12})^2 + 4(\rho_{10,11} + \rho_{4,5})^2} \right).$$

Besides, the eigenvalue of the partially transposed reduced density matrix $\rho_{ac}^{\text{T}_c}$ that constitutes bipartite negativity N_{ac} would be expressed by:

$$\lambda_1 = \rho_{2,2} + \rho_{4,4} + \rho_{6,6}, \quad \lambda_2 = \rho_{7,7} + \rho_{9,9} + \rho_{11,11},$$

and

$$\lambda_{3;4} = \frac{1}{2} \left(\rho_{1,1} + \rho_{3,3} + \rho_{5,5} + \rho_{8,8} + \rho_{10,10} + \rho_{12,12} \pm \sqrt{(\rho_{1,1} + \rho_{3,3} + \rho_{5,5} - \rho_{8,8} - \rho_{10,10} - \rho_{12,12})^2 + 4(\rho_{2,7} + \rho_{4,9} + \rho_{6,11})^2} \right)$$

[1] R. Horodecki, P. Horodecki, M. Horodecki, and K. Horodecki, *Rev. Mod. Phys.* **81**, 865 (2009).

[2] R. L. Carlin, *Magnetochemistry* (Springer, Berlin, 1986).

- [3] O. Kahn, *Molecular Magnetism* (Wiley, New York, 1993).
- [4] M. C. Arnesen, S. Bose, and V. Vedral, *Phys. Rev. Lett.* **87**, 017901 (2001).
- [5] L. Amico, R. Fazio, A. Osterloh, and V. Vedral, *Rev. Mod. Phys.* **80**, 517 (2008).
- [6] C. Benelli, D. Gatteschi, *Introduction to Molecular Magnetism*, (Wiley-VCH: Weinheim, Germany 2015).
- [7] A. Tribedi and I. Bose, *Phys. Rev. A* **74**, 012314 (2006).
- [8] F. Troiani and M. Affronte, *Chem. Soc. Rev.* **40**, 3119 (2011).
- [9] H. Čenčariková and J. Strečka, *Phys. Rev. B* **102**, 184419 (2020).
- [10] H. Vargová, J. Strečka, *Results Phys.* **61**, 107728 (2024).
- [11] W. H. Zurek, *Rev. Mod. Phys.* **75**, 715 (2003).
- [12] S. Kanai, F. J. Heremans, H. Seo, G. Wolfowicz, C. P. Anderson, S. E. Sullivan, M. Onizhuk, k G. Galli, D. D. Awschalom, and H. Ohno, *PNAS* **119**, e2121808119 (2022).
- [13] L. Gassab, O. Pusuluk, and Ö. E. Müstecaplıođlu, *Phys. Rev. A* **109**, 012424 (2024).
- [14] M. Kitagawa and M. Ueda, *Phys. Rev. A* **47**, 5138 (1993).
- [15] M. Reboiro, O. Civitarese, and L. Rebon, *Phys. Lett. A* **366**, 241 (2007).
- [16] M. Jafarpour and A. Akhound, *Phys. Lett. A* **372**, 2374 (2008).
- [17] J. Ma, X. Wang, C. P. Sun, and F. Nori, *Phys. Rep.* **509**, 89 (2011).
- [18] R. Schmied, *Spin squeezing as a probe of many-body quantum correlations*, (PhD thesis, University of Basel, Switzerland, 2016).
- [19] S. Mahdaviifar, F. K. Fumani, B. Haghdoost, M. R. Soltani, [arXiv:2401.12500v1](https://arxiv.org/abs/2401.12500v1).
- [20] X. Wang, *Opt. Comm.* **200**, 277 (2001).
- [21] L. Jaeger, *The Second Quantum Revolution*. (Springer Nature, Baar, Switzerland 2018).
- [22] H. Bao, J. Duan, S. Jin, *et al.*, *Nature* **581**, 159 (2020).
- [23] M. Calixto, A. Mayorgas, and J. Guerrero, *Quant. Inf. Process.* **20**, 304 (2021).
- [24] S. Sinha, J. Emerson, N. Boulant, E. M. Fortunato, T. F. Havel, and D. G. Cory, *Quant. Inf. Process.* **2**, 433 (2003).
- [25] W. Wasilewski, K. Jensen, H. Krauter, J. J. Renema, M. V. Balabas, and E. S. Polzik, *Phys. Rev. Lett.* **104**, 133601 (2010).
- [26] R. J. Sewell, M. Koschorreck, M. Napolitano, B. Dubost, N. Behbood, and M. W. Mitchell, *Phys. Rev. Lett.* **109**, 253605 (2012).
- [27] H. Bao, S. Jin, J. Duan, S. Jia, K. Mølmer, H. Shen, and Y. Xiao, *Nat. Commun.* **11**, 5658 (2020).
- [28] T. Baumgratz, M. Cramer, and M. B. Plenio, *Phys. Rev. Lett.* **113**, 140401 (2014).
- [29] M. Schlosshauer, *Rev. Mod. Phys.* **76**, 1267 (2005).
- [30] M. Schlosshauer, *Phys. Rep.* **831**, 1 (2019).
- [31] A. Streltsov, G. Adesso, and M. B. Plenio, *Rev. Mod. Phys.* **89**, 041003 (2017).
- [32] M. L. Hu, X. Hu, J. Wang, Y. Peng, Y. R. Zhang, and H. Fan, *Phys. Rep.* **762–76**, 1 (2018).
- [33] Z.-H. Ma, J. Cui, Z. Cao, S.-M. Fei, V. Vedral, T. Byrnes, and C. Radhakrishnan, *EPL* **125**, 50005 (2019).
- [34] D. P. DiVincenzo and D. Loss, *J. Magn. Magn. Mater.* **200**, 202 (1999).
- [35] M.-L. Hu and H. Fan, *Ann. Phys.* **327**, 851 (2012).
- [36] Z. Xi, Y. Li, and H. Fan, *Sci. Rep.* **5**, 10922 (2015).
- [37] D. J. Wineland, J. J. Bollinger, W. M. Itano, and D. J. Heinzen, *Phys. Rev. A* **50**, 67 (1994).
- [38] X. Wang and B. C. Sanders, *Phys. Rev. A* **68**, 012101 (2003).
- [39] H. M. Wiseman and G. Milburn, *Quantum Measurement and Control* (Cambridge Univ. Press, 2010).
- [40] L. Shao, L. Fu, *Phys. Rev. A* **109**, 052618 (2024).
- [41] A. Sørensen and K. Mølmer, *Phys. Rev. Lett.* **83**, 2274 (1999).
- [42] M. Ö. Oktel, Ö. E. Müstecaplıođlu, *Laser Phys.* **19**, 625 (2009).
- [43] D. Wellnitz, M. Mamaev, T. Bilitewski, and A. M. Rey, *Phys. Rev. Research* **6**, L012025 (2024).
- [44] J. A. Hines, S. V. Rajagopal, G. L. Moreau *et al.* *Phys. Rev. Lett.* **131**, 063401 (2023).
- [45] M. A. Perlin, C. Qu, and A. M. Rey, *Phys. Rev. Lett.* **125**, 223401 (2020).
- [46] V. Giovannetti, S. Lloyd, and L. Maccone, *Phys. Rev. Lett.* **96**, 010401 (2006).
- [47] V. Giovannetti, S. Lloyd, and L. Maccone, *Nat. Photonics* **5**, 222 (2011).
- [48] L. Pezzè, A. Smerzi, M. K. Oberthaler, R. Schmied, and P. Treutlein, *Rev. Mod. Phys.* **90**, 035005 (2018).
- [49] J. Ma, X. Wang, C.P. Sun, and F. Nori, *Phys. Rep.* **509**, 89 (2011).
- [50] B. Braverman, A. Kawasaki, E. P. Peñafiel *et al.*, *Phys. Rev. Lett.* **122**, 223203 (2019).
- [51] D. J. Wineland, J. J. Bollinger, W. M. Itano, and D. J. Heinzen, *Phys. Rev. A* **46**, R6797 (1992).
- [52] D. U. Orgikh and M. Kitagawa, *Phys. Rev. A* **64**, 052106 (2001).
- [53] R. J. Birrittella, J. Ziskind, E. E. Hach, P. M. Alsing, and C. C. Gerry, *J. Opt. Soc. Am. B* **38**, 3448 (2021).
- [54] W. Huang, X. Liang, B. Zhu, Y. Yan, C. H. Yuan, W. Zhang, L. Chen, *Phys. Rev. Lett.* , **130**, 073601 (2023).
- [55] A. André, A. S. Sørensen, and M. D. Lukin, *Phys. Rev. Lett.* **92**, 230801 (2004).
- [56] W. J. Eckner, N. D. Oppong, A. Cao, *et al.*, *Nature* **621**, 734 (2023).
- [57] A. Biswas, M. Ghosh, P. Lemoine, S. Sarkar, S. Hazra, and S. Mohanta, *Eur. J. Inorg. Chem.* **20**, 3125 (2010).
- [58] S. b. Wang, R. f. Li, G. m. Yang, D. Z. Liao, Z. H. Jiang, and S. P. Yan, *Inorgan. Chim. Act.* **358**, 2595 (2005).
- [59] N. Hari, S. Mandal, A. Jana, H. A. Sparkesb and S. Mohanta, *RSC Adv.* **8**, 7315 (2018).
- [60] Z. Adamyán and V. Ohanyan, [arXiv:2405.00178](https://arxiv.org/abs/2405.00178).
- [61] G. Vidal and R. F. Werner, *Phys. Rev. A* **65**, 032314 (2002).
- [62] A. Peres, *Phys. Rev. Lett.* **77**, 1413 (1996).
- [63] C. Sabín and G. García-Alcaine, *Eur. Phys. J. D* **48**, 435 (2008).
- [64] A. Streltsov, U. Singh, H. S. Dhar, M. N. Bera, and G. Adesso, *Phys. Rev. Lett.* **115**, 020403 (2015).
- [65] J. R. Johansson, P. D. Nation, and F. Nori, *Comput. Phys. Commun.* **183**, 1760 (2012).
- [66] J. R. Johansson, P. D. Nation, and F. Nori, *Comput. Phys. Commun.* **184**, 1234 (2013).